Transp Porous Med (2010) 82:93–109
DOI 10.1007/s11242-009-9426-x

An Experimental Study on the Influence of Sub-Core Scale Heterogeneities on CO_2 Distribution in Reservoir Rocks

Jean-Christophe Perrin · Sally Benson

Received: 5 February 2009 / Accepted: 1 June 2009 / Published online: 30 June 2009

Abstract This article presents the results of CO_2/brine two-phase flow experiments in rocks at reservoir conditions. X-ray CT scanning is used to determine CO_2 saturation at a fine scale with a resolution of a few pore volumes and provide 3D porosity and saturation maps that can be use to correlate CO_2 saturations and rock properties. The study highlights the strong influence of sub-core scale heterogeneities on the spatial distribution of CO_2 at steady state and provides useful relative permeability data on a sample originated from an actual storage site (CO2CRC-Otway project, Victoria, South-West Australia). Two different samples tested, although different in nature, present strong heterogeneities, but differ in the detail of the connectivity of high porosity layers. In both samples, the results of the investigations show that sub-core scale heterogeneities control the sweep efficiency and may cause channeling through the porous medium. In one of the samples, CO_2 saturation appears uncorrelated to porosity close to the outlet end of the core. This observation is understood as a result of the position and the orientation of high porosity layers with respect to the inlet face of the core. Finally, in the operating conditions of the two experiments, the saturation maps demonstrate that gravity does not play a major role since no detectable buoyancy driven flow is observed.

Keywords Carbon capture and sequestration · Relative permeability · X-ray CT scanning · Heterogeneity · Flow through porous media · Drainage

1 Introduction

Among the different main types of potential storage formations (saline aquifers, depleted oil reservoirs, unminable coal seams), saline aquifers have by far the largest estimated storage capacity and are more broadly distributed worldwide. In order to improve our understanding

J.-C. Perrin (✉) · S. Benson
Department of Energy Resources Engineering, Stanford University, Green Earth Sciences Bldg. #069, 367 Panama Street, Stanford, CA 94305, USA
e-mail: perrin@stanford.edu

of multi-phase flow and trapping in CO_2-brine systems and take advantage of this capacity, more experimental data, numerical simulations, and theoretical studies are needed. While the literature describing multi-phase flow of oil and water, and CO_2 and oil is abundant, very few laboratory experiments have been performed on CO_2/brine systems (Bennion et al. 2005, 2006a,b,c; Benson et al. 2006; Shi et al. 2009; Tetsuya et al. 2008; Perrin et al. 2009) and, thus, very few data available.

In multi-phase flow, the concept of relative permeability is fundamental when one has to predict the spatial and temporal distribution of CO_2 saturation and trapping, migration of the CO_2 plume, or the injection pressure. Relative permeability curves to CO_2 and brine can be measured in the laboratory but the validity of using laboratory-measured relative permeability curves to describe the reservoir is subject to a number of uncertainties. The fact that nearly all the samples that are investigated in the lab are heterogeneous (Huppler 1970) and that these heterogeneities are not representative of the full range of heterogeneities in the reservoir are strong source of uncertainty. As noted by a number of authors, relative permeability is indeed dependent on the wettability of the rock (Caruana and Dawe 1996), flow directions (Honarpour et al. 1986; Crotti et al. 1998), and heterogeneities (Crotti et al. 1998). All these factors can be different in the lab and in the field, either because the rock sample investigated can have different properties (wettability), the way the experiments are performed does not coincide with the actual injection (flow directions) or because the heterogeneities of the lab sample are not representative of the reservoir.

Understanding the role of heterogeneities on the distribution of CO_2 in rock samples at the core and sub-core levels provides a first step toward a better understanding of the phenomena leading to a dependence of the relative permeability curves on heterogeneities and toward appropriate methods for up scaling laboratory-measured data to simulate field-scale multi-phase flow behavior.

In this article, we present two sets of steady-state multi-phase flow experiments that are performed using an apparatus that allows continuous injection of CO_2 and brine in a core sample maintained at reservoir pressure and temperature. X-ray CT scanning is used to determine porosity and CO_2 saturation at a fine resolution corresponding to the volume of several pores. Two main objectives are pursued: (1) to provide some experimental data measured on a rock sample from an actual storage site and (2) to visualize and understand the effect of core and sub-core scale heterogeneities on CO_2 saturation distributions and relative permeability.

2 Materials and Methods

2.1 Description of the Core Flooding Experimental Setup

In this section, we describe the experimental setup that has been designed and used for the investigation of two-phase core flooding experiments (Fig. 1). The rock sample is wrapped in a heat-shrinkable Teflon sleeve and placed in an aluminum core holder. A displacement pump (Teledyne Isco, Model 260D/Pump D in Fig. 1) injects water around the sleeve to create the overburden pressure (reservoir pressure, P_{res}). Two electric heaters heat the water inside the core holder to maintain the core at the reservoir temperature (T_{res}). P_{res} and T_{res} mimic the pressure and temperature experienced by the reservoir rock in a typical storage project. They are both kept constant during an experiment. Two dual-pump systems are used to inject brine and CO_2 in the core sample (Teledyne Isco, Model 500D/Pump A1 and A2 for CO_2, and B1 and B2 for brine. The pumps have an accuracy of 0.5% of the setpoint). Both systems are

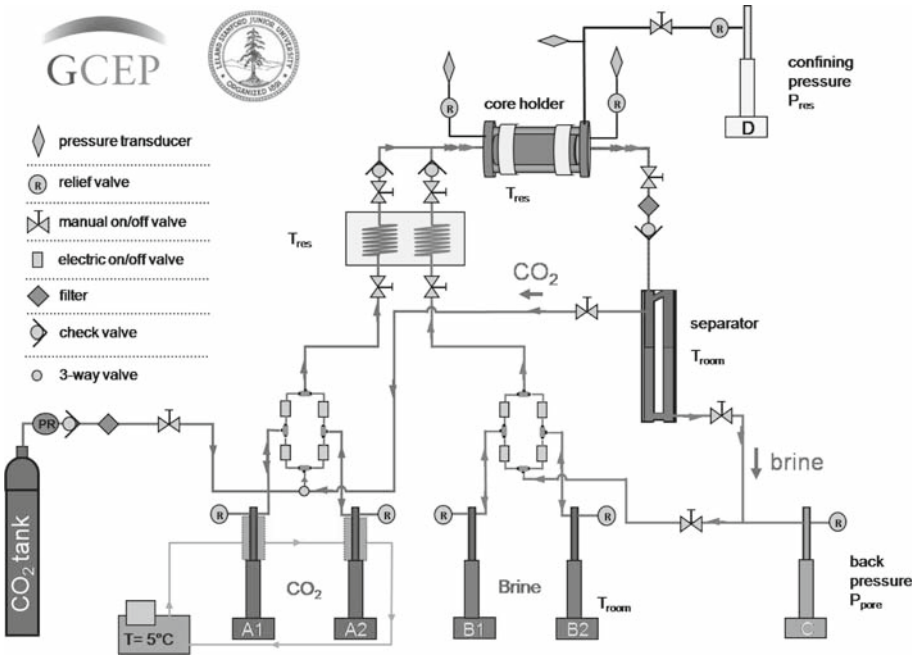

Fig. 1 Experimental setup developed for two-phase core flooding experiments. During the injection the core sample is maintained at reservoir temperature and reservoir pressure. CO_2 and brine circulate in a closed loop and saturation images are obtained using CT scanning

composed of two pumps connected with a set of electric valves. The dual-pump configurations provide continuous fluid delivery by synchronizing the pump and refill strokes so that at least one pump is always delivering fluid. Electric valves support automated functions.

The bodies of the CO_2 pumps are surrounded by water-cooled temperature jackets to keep CO_2 at a constant temperature of 5°C, which allows fast and complete filling and refilling of the cylinder when pumping the liquefied fluid. Before entering the core, CO_2 and brine pass through a water bath (heat exchanger) to be heated to T_{res}. The two fluids are then mixed and co-injected into the core. After flowing through the core, CO_2 and brine are separated by gravity in a high pressure separator composed of a high pressure vessel adjacent to a heavy-duty high pressure liquid level gage. The liquid level gage is equipped with a transparent 1/2 inch thick glass which allows measurement of the height of the interface between brine and liquid CO_2 during the experiment. After the separator, the CO_2 returns back to the CO_2 pump system and the brine returns back to the brine pump system. Between the separator and the brine pump system, another pump (Teledyne Isco, Model 1000D/Pump C) is used to maintain the back pressure in the system. The back pressure, also called pore pressure, is always set at least 200 psi (∼1.4 MPa) below the overburden pressure value to avoid fluid leakage through the Teflon sleeve surrounding the core. This pump is used as a buffer volume as well. While it is possible for CO_2 to diffuse through the Teflon sleeve, the effect of this on the experiments is not significant because the saturation images and pressure gradients are measured at steady state while the fluids are injected at rates far in excess of the rate of diffusion (diffusion rates have been independently measured in a static system and shown to be slow, resulting in a net loss of CO_2 saturation on the order of 1–2% over a day). Owing to the use of dual-pump systems, CO_2 and brine circulate continuously in the system. Thus, the

two fluids are in constant contact each other, ensuring that the CO_2 and brine are in equilibrium with each other prior to injecting the fluids into the core. This precaution is intended to avoid any drying of the core, which is often encountered when dry CO_2 is used for injection. Before the beginning of each experiment, CO_2 and brine are circulated through the system for about one day to pre-equilibrate the fluids. The two fluids are in contact in the tubing and in the separator. The separator allows observation of the height of the interface between CO_2 and brine. When this height is stable, the fluids are in equilibrium. In addition, the measured volume of CO_2 that dissolves into the brine equals that which would be expected at the imposed pressure and temperature.

2.2 Data Collection

During the experiment, the pressure at the inlet and outlet ends of the core is measured with two high accuracy pressure transducers (Oil filled Digiquartz ® Intelligent Transmitter, Model 9000-3K-101). The difference in the values between the two pressures gives the pressure drop across the core which is used to calculate the absolute permeability of the rock sample when only one fluid is flowing and the relative permeability to each fluid when both CO_2 and brine are injected. The two transducers are calibrated against each other before each run to ensure accurate differential pressure measurements. Direct measurements of CO_2 and brine phase pressures are not measured independently. The temperature inside the core holder, the pressure drop, the injection flow rate, the injection pressure, and the volume of each pump are measured and recorded by a data acquisition system. X-ray CT scanning is used to determine CO_2 and brine saturations, in real time, inside the core sample. The procedure used for the saturations measurements is described in the following paragraph.

2.3 Methods

2.3.1 Relative Permeability Measurements

Steady-state relative permeability experiments are performed using the setup described before.

The samples are 2-inch (5.08 cm) diameter cylinders, with a length in the range 2.5–8 inches. (6.35–20.32 cm). The samples were fired at 600°C for 17 h to stabilize clays and avoid any unwanted swelling or chemical reactions. The average absolute permeability of the core is first measured by injecting brine at different constant flow rates and measuring the pressure drop across the core sample corresponding to each rate. Using Darcy's law and knowing the viscosity of the brine solution at the experimental conditions (T_{res}, P_{res}), the permeability is easily determined with a precision of 2–5%.

In order to measure a drainage relative permeability curve CO_2 and brine are co-injected in different proportions (different fractional flows). The core is initially completely brine saturated and fractional flows of CO_2 are increased progressively to a fractional flow of 100% CO_2. In order to ensure that the core is fully saturated with brine before the experiment begins, the core is first dried and scanned. Then CO_2 is injected at atmospheric pressure at a low flow rate for about 12 h to remove all of the air from the core. A few pore volumes of brine are then injected at low flow rate to displace most of the CO_2 through a combination of displacement and dissolution. Any remaining separate phase CO_2 is dissolved into the brine by increasing the pressure to reservoir conditions. Verification that brine saturation has been achieved is checked before the experiments using the CT scanner.

The fractional flow of CO_2 f_{CO_2} is defined as the ratio between the volumetric flow rate of brine-saturated CO_2 at reservoir conditions $\mathrm{FR}_{CO_2}^{T_{res},P_{res}}$ and the total volumetric flow rate $\mathrm{FR}_{CO_2}^{T_{res},P_{res}} + \mathrm{FR}_{brine}^{T_{res},P_{res}}$:

$$f_{CO_2} = \frac{\mathrm{FR}_{CO_2}^{T_{res},P_{res}}}{\mathrm{FR}_{CO_2}^{T_{res},P_{res}} + \mathrm{FR}_{brine}^{T_{res},P_{res}}} \tag{1}$$

When an injection is performed, the flow rate is set directly as one of the pump's parameters. Since the temperature of the fluids vary between the pumps (5°C for CO_2, room temperature for brine) and the heat exchanger (T_{res}), the fluids properties, and, in particular, the density of CO_2 (d_{CO_2}) associated with its liquid/supercritical phase change, vary as well. For example, the ratio

$$\frac{d_{CO_2}^{5°C,1800\,\mathrm{psi}}}{d_{CO_2}^{50°C,1800\,\mathrm{psi}}}$$

is as high as 1.583, meaning that a flow rate of CO_2 of 1 cm^3/min at 5°C and 1,800 psi (12.41 Mpa) becomes 1.583 cm^3/min at 50°C and the same pressure conditions. This important density change must be taken into account when calculating the fractional flows. For each given fractional flow, the pressure drop across the core is measured as well as the CO_2 saturation in the core. At steady state, when the saturation distribution and pressure drop have stabilized, the data sets used for relative permeability measurements are collected. Steady state is generally reached after having injected 3–5 pore volumes of fluids and the data are always collected after at least six pore volumes.

The fractional flow of CO_2 is then progressively increased and the relative permeability is determined for each step. The procedure is repeated until 100% of CO_2 is injected. The relative permeability curves consist of a plot of the relative permeability to CO_2 and brine as a function of the core-averaged brine saturation.

2.3.2 Determination of Porosity and CO_2 Saturation at the Sub-Core Scale

A medical X-ray CAT scanner is used to map porosity and CO_2 saturation in the core during the experiment. This technique, although relatively new, is now widely used in petroleum engineering labs (Schembre and Kovscek 2003; Shi et al. 2009). The scanner creates 2-D images at different locations along the length of the sample. The 3-D maps are then constructed by stacking the 2-D images along the third dimension. The *X–Y* resolution in the plane is 0.254 mm × 0.254 mm for the experiments that are discussed here. The slice thickness is either 1 or 3 mm, depending on the experiment.

In order to obtain the porosity map of a core, two sets of images are needed: the dry images, when the sample is dry and the pore space is filled with air, and the brine saturated images, when the core is fully saturated with brine at the reservoir conditions. The porosity Φ of each voxel element is then calculated using (Akin and Kovscek 2003):

$$\Phi = \frac{\mathrm{CT}_{brine}^{sat} - \mathrm{CT}_{dry}}{\mathrm{CT}_{brine} - \mathrm{CT}_{air}} \tag{2}$$

where CT is a numerical value converted from the X-ray attenuation coefficients. The CT numbers are normalized values relative to the linear absorption coefficient of water (Wellington and Vinegar 1987).

Table 1 Sample properties and experimental conditions—sample #1

Sample properties	Experimental conditions	
Sample #1 (Well CRC1 -2071m CO2CRC-Otway project, Australia)		
$\bar{\Phi} = 0.182$	$T_{res} = 63°C$	Brine composition: Na, 2,390 ppm; Cl, 4,013 ppm; Ca, 183 ppm
$\bar{k} = 45 \pm 2$mD	$P_{res} = 12.4$ MPa	
$L = 8.3$ cm	Voxel size = 0.2539 × 0.2539 × 1 mm	Total flow rate: 2 ml/min (corresponding to a capillary number of Ca $\sim 2.5 \times 10^{-5}$ and gravity number of $G = 0.033$)
Ø = 5.08cm		

The capillary number is calculated using $\text{Ca} = \mu U/\sigma$ where μ is the brine viscosity, U is the fluid velocity and σ (30 mN/m) is the interfacial tension between brine and CO_2. The gravity number, G, is calculated using $G = \bar{k}\Delta\rho g/\mu U$, where $\Delta\rho$ is the difference in density between brine and CO_2

In order to obtain the saturation map at each CO_2 fractional flow, three sets of images are needed: the brine saturated images, the CO_2-saturated images (the core is filled with CO_2 at reservoir conditions) and the experimental images, at steady state, for the corresponding fractional flow. The CO_2 and brine saturations are then calculated for each voxel using (Akin and Kovscek 2003):

$$S_{CO_2} = \frac{\text{CT}_{\text{exp}} - \text{CT}^{\text{sat}}_{\text{brine}}}{\text{CT}^{\text{sat}}_{CO_2} - \text{CT}^{\text{sat}}_{\text{brine}}} \quad \text{and} \quad S_{\text{brine}} = 1 - S_{CO_2} \tag{3}$$

3 Experimental Results: Influence of Heterogeneities on the Distribution of CO_2 Saturation

3.1 Sample #1: Large Heterogeneities Perpendicular to the Flow Direction

The first experiment was performed on a sample that was cored from the CRC1 well of the CO2CRC-Otway project in the south west part of Australia. The measured properties of the sample as well as the experimental conditions that were chosen for the measurement of the relative permeability curves during the drainage phase are reported in Table 1. The total injection rate (2 ml/min ↔ 7.8 m/day) corresponds to the fluid velocity that would be expected for a large CO_2 storage project in the region near the injection well. The 3D maps of the core porosity and CO_2 saturation were obtained by recording 77 consecutive images, each one being 1 mm thick.

Figure 2 shows the slice-averaged porosity profile along the core (Fig. 2a) and the 3D view of the porosity map (Fig. 2b). The porosity demonstrates stratigraphic variations along the core with a high degree of variability along the length of the core. As revealed by the 3D view, several low porosity layers with a small dip angle (positions 5–6 and 53–54 in the profile and light blue colors in the 3D map) are present.

The steady-state three-dimensional views of CO_2 saturation in the core at different CO_2 fractional flows are shown in Fig. 3. The slice-averaged CO_2 saturation profile in the $f_{CO_2} = 1$ case is plotted Fig. 4, together with the porosity profile.

From the observation of these two figures we can note that

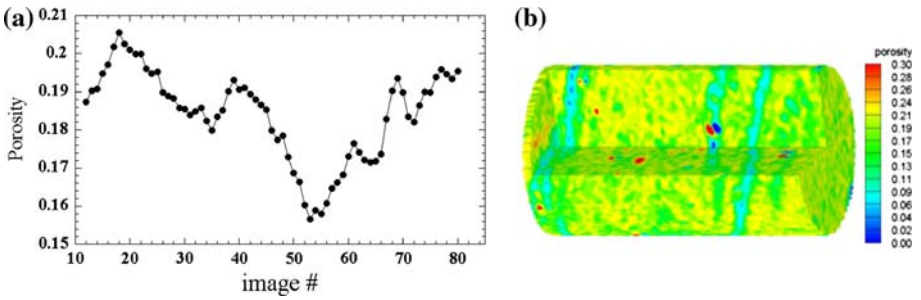

Fig. 2 Sample #1. **a** Porosity profile along the core. **b** Three dimensional porosity map

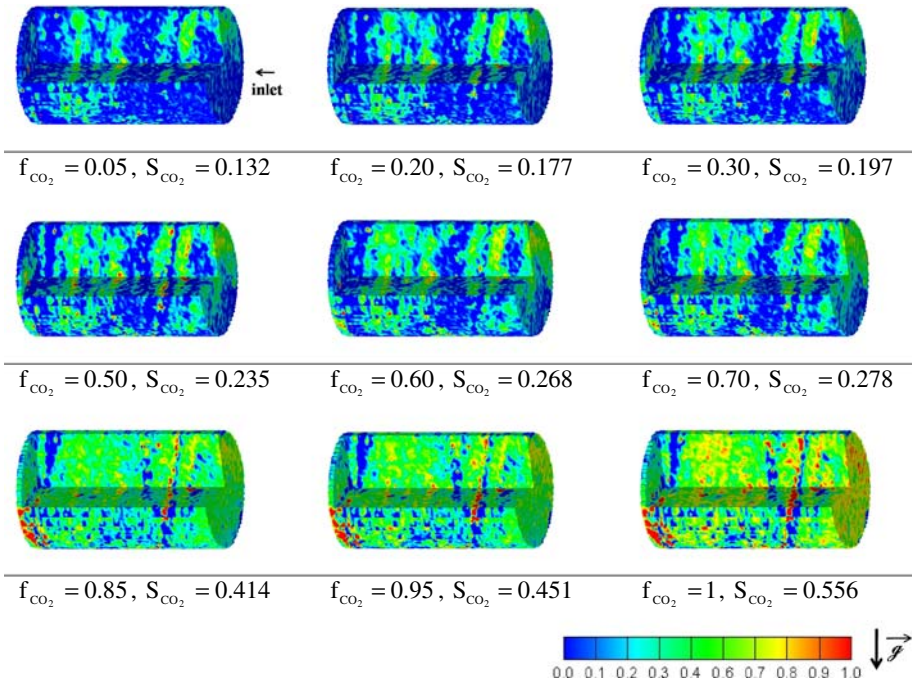

Fig. 3 Three dimensional maps of CO_2 saturation inside the rock sample at steady state for different fractional flows of CO_2. The CO_2 saturation S_{CO_2} is indicated below each image together with the corresponding fractional flow. The views show the core in its real orientation during the experiment, the gravity being oriented from top to bottom. The fluids are injected from right to left as indicated by the arrow at the right side of the 5% CO_2 fractional flow case

- Variability of CO_2 saturation along the core is significant;
- Spatial distribution of CO_2 inside the core is very heterogeneous and the steady-state saturation distributions mimic the stratigraphic features observed in the porosity map;
- Low porosity layers correspond to low CO_2 saturation and higher porosity regions have higher average CO_2 saturation;
- No important end effects are visible since no visible general trend is seen close to the ends of the core;

- No obvious signs of gravity override of the less dense CO_2 phase are observed, either at the inlet or along the length of the core.

The last two observations are supported by the fact that the porosity and the CO_2 saturation profiles have the same trends along the length of the core, even close to the end sections. The capillary end effect, when present, results from a discontinuity in capillary pressure at the ends of the core, tends to make it more difficult for the wetting phase than for the non-wetting phase to leave the porous media and results in a buildup of the wetting phase at the efflux end of the system. If capillary end effects were important during these experiments, then there would be a decrease in the CO_2 saturation that is uncorrelated with the rock properties (Honarpour et al. 1986), which is not observed.

The correlation between porosity and saturation is easily visualized when plotting the slice-averaged CO_2 saturation as a function of the slice-averaged porosity for several different CO_2 fractional flows (Fig. 5). From this set of curves we see that, for each fractional flow, the CO_2 preferentially occupies the regions of the core where porosity is the highest.

At the sub-core scale, the correlation porosity–saturation is illustrated in Fig. 6, where the 2D maps of the core porosity and CO_2 saturation are shown for slices that were taken at positions 26, 33 and 75. As indicated in Fig. 4, position #1 corresponds to the outlet of the core and position #77 to the inlet. The match between the spatial distribution of porosity and CO_2 saturation is striking even if the pixel by pixel correlation is poor due to scattering of the data.

In order to make a more consistent comparison between the slice averaged properties and the pixel by pixel properties, the regression lines of the curves CO_2 saturation versus porosity are plotted in Fig. 7 at $f_{CO_2} = 1$ for images captured every 5 mm along the core, together with the line corresponding to slice averaged correlation.

The lines are parallel to each other along the length of the sample, even close to the ends. Thus, the correlation stays identical at each position which confirms the absence of end effects. The good correlation between all of the regression lines also suggests that the relationship between saturation and porosity is fairly uniform over the entire core. Most importantly, the

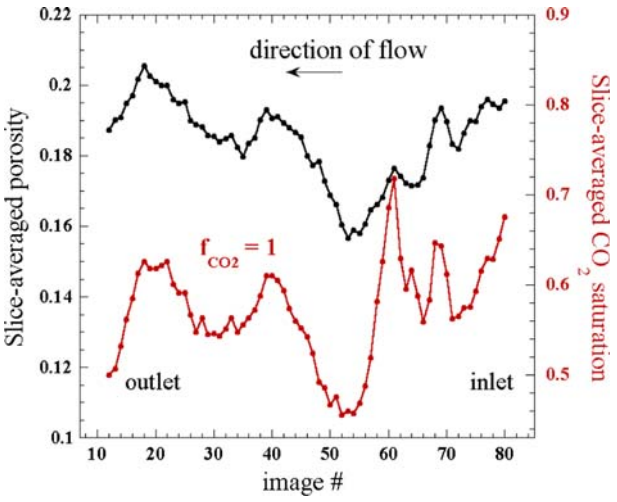

Fig. 4 Slice-averaged CO_2 saturation profile corresponding to the $f_{CO_2} = 1$ case and porosity profile along the core. The same trends are observed in the two profiles. No end effects are visible in the CO_2 profile

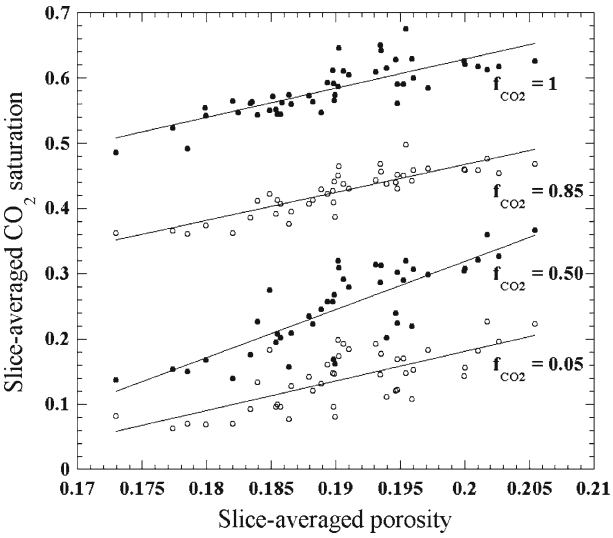

Fig. 5 Correlation between the slice-averaged CO_2 saturation values and the slice-averaged porosity for different fractional flows of CO_2. The R^2 values of the regression lines are ranging between 0.65 and 0.8

consistency of these correlations suggests that there is a fundamental relationship between the porosity of the rock and CO_2 saturation that could be exploited to improve understanding of the physical controls on multi-phase flow of CO_2 and brine.

In Fig. 8, porosity (a) and saturation of slice #33 are shown for $f_{CO_2} = 0.3$ (b) and $f_{CO_2} = 1$ (c). In Fig. 8a′–c′, the same images are represented in a color scale that displays in red the porosity values that are greater than 0.2 (a′) and the CO_2 saturation values that are greater than 0.65 [b′ for $f_{CO_2} = 0.3$ and c′ for $f_{CO_2} = 1$]. Figure 7d–f and d′–f′ correspond, respectively, to details of a–c and a′–c′. The detailed views e and e′ clearly show that, when the proportion of CO_2 is low (beginning of the drainage), CO_2 tends to occupy first the areas of high porosity.

Figure 9 presents the relative permeability curves measured at the conditions described before together with the experimental data. As a result of the inhomogeneous distribution of CO_2 in the core due to the presence of heterogeneity, the residual brine saturation is high (0.44) as compared to the oil industry standards (Honarpour et al. 1986) but is in the range of what is measured for CO_2 and brine (Bennion et al. 2005).

3.2 Sample #2: Moderate Heterogeneities Sub-Parallel to the Flow Direction

The second experiment described in this article was performed on a core of Berea sandstone. The measured properties of the sample as well as the experimental conditions that were chosen for the measurement of the relative permeability curves during the drainage phase are reported in Table 2. The 3D maps of the core porosity and CO_2 saturation were obtained by recording 29 images in the first case that is described [sample #2 (a)] and 151 consecutive images in the second case [sample #2 (b)]. The two cases, referred as (a) and (b) are both drainage experiments, performed in the exact same experimental conditions and using the same procedure, except for two important points:

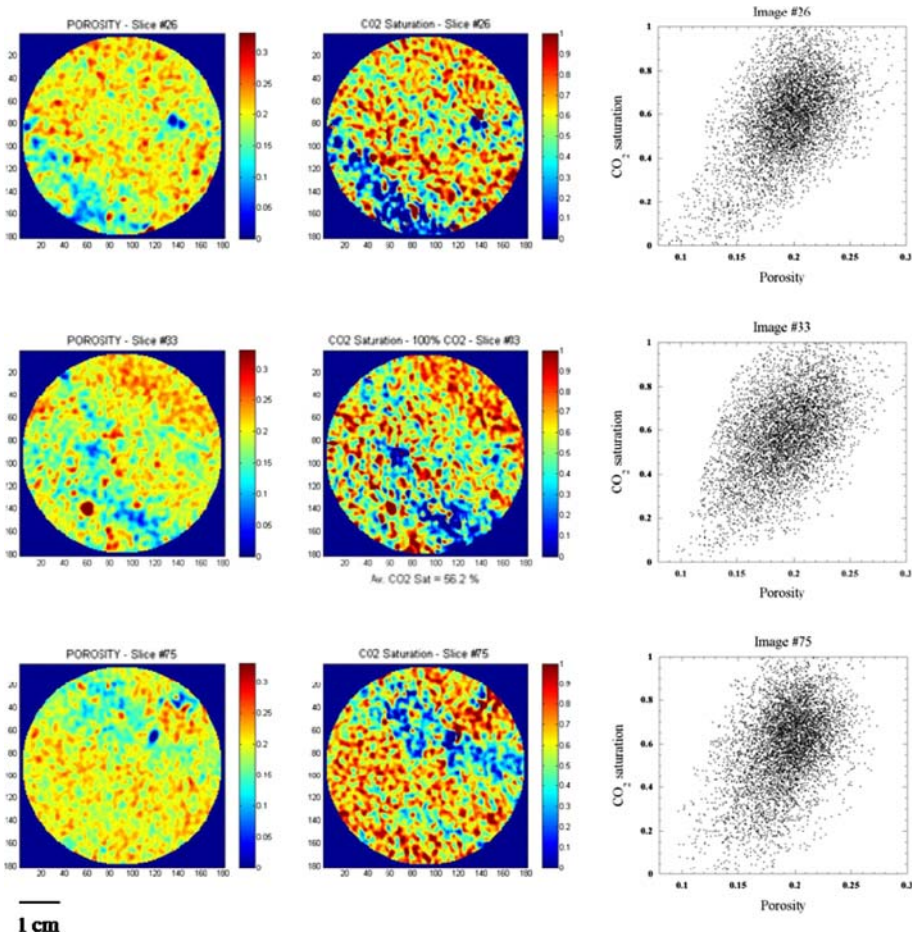

Fig. 6 Visual comparison and pixel by pixel correlation between porosity and CO_2 saturation for the $f_{CO_2} = 1$ case at three different locations along the core (images #26, #33 and #75)

- Experiment (b) was performed after having rotated the core sample 180° along its main axis, this allowed us to distinguish the effects of heterogeneity from potential gravity effects;
- The slice thickness was 3 mm with an interval of 2.08 mm between two images in experiment (a) and 1 mm with no interval between two consecutive images in (b). The voxel size is thus about five times smaller in experiment (b).

The slice-averaged CO_2 saturation profile obtained during experiment (a) in the $f_{CO_2} = 1$ case is plotted Fig. 10, together with the porosity profile. In Fig. 11, the 3D porosity map is shown together with the CO_2 saturation maps obtained during both experiments at $f_{CO_2} = 1$.

A few remarks can be made based on the observation of the porosity profile and the porosity map:

- Although the slice-averaged porosity profile is quite uniform on average, the 3D porosity map illustrates some important sub-core scale heterogeneities;
- The bedding can be seen going through the core with a high dip angle; and

- Some higher porosity layers are not connected to the inlet face of the core.
- From the comparison of the porosity profile and the saturation profile and the observation of the distribution of CO_2 saturation in the core we can conclude that
  - The correlation between porosity–saturation is good close to the inlet face of the core and in the first two-thirds of the sample. The correlation is lost close to the outlet end of the core;
  - The lost of correlation close to the outlet end of the core is not attributed to a capillary end effect or gravity, but due to a heterogeneity effect. The regions that are mostly saturated with brine close to the outlet are isolated from the inlet face of the sample by low porosity layers. This observation can also be understood as a result of a channeling through the more permeable (higher porosity) areas causing an early breakthrough. The low porosity layers act as a capillary barrier, preventing the lateral flow across them, which would be needed to displace brine from the portions of the core that are isolated from the inlet by the low porosity layers.
  - The change of orientation of the core between experiment (a) and (b) does not change the overall distribution of CO_2 in the sample. The only visible differences are due to the two different resolutions. Thus, the lost of correlation close to the outlet of the core is not due to any kind of gravity effect.

Figure 12 shows the porosity and saturation images measured close to the inlet face [(a), slice #143 and (b), slice #29] and close to the outlet [(a), slice #7 and (b), slice #2]. As noted above, the spatial distribution of CO_2 saturation presents the same features as porosity close to the inlet but is not correlated to porosity anymore close to the outlet. Also, the distribution of CO_2 is not correlated to the direction of the gravity vector.

Figure 13 presents the relative permeability curves that were measured during experiment (a). As in the case of sample #1, the residual brine saturation is high (0.62) as the result of the bypassing of a large portion of the core sample by CO_2. In this second case, however, the effect is enhanced by the spatial orientation of the bedding of the rock. Because the heterogeneities of this rock sample and their relative disposition with respect to the axis of the

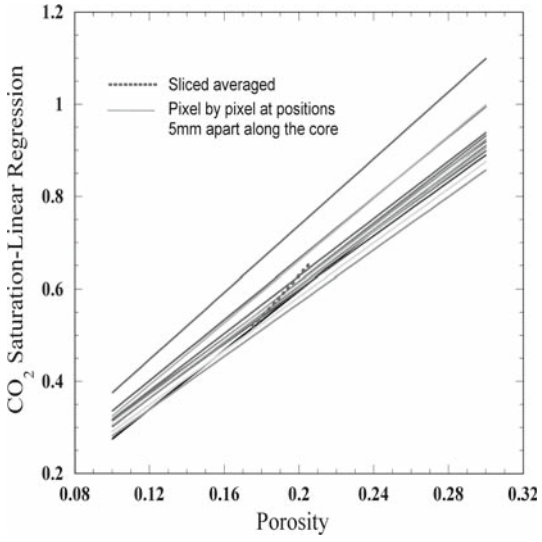

Fig. 7 Regression lines of the curves CO_2 saturation versus porosity at $f_{CO_2} = 1$ for images taken every 5 mm along the core (*continuous lines*) and regression line corresponding to the slice-averaged correlation (*dotted line*). The R values of the regression lines are within (0.42–0.58)

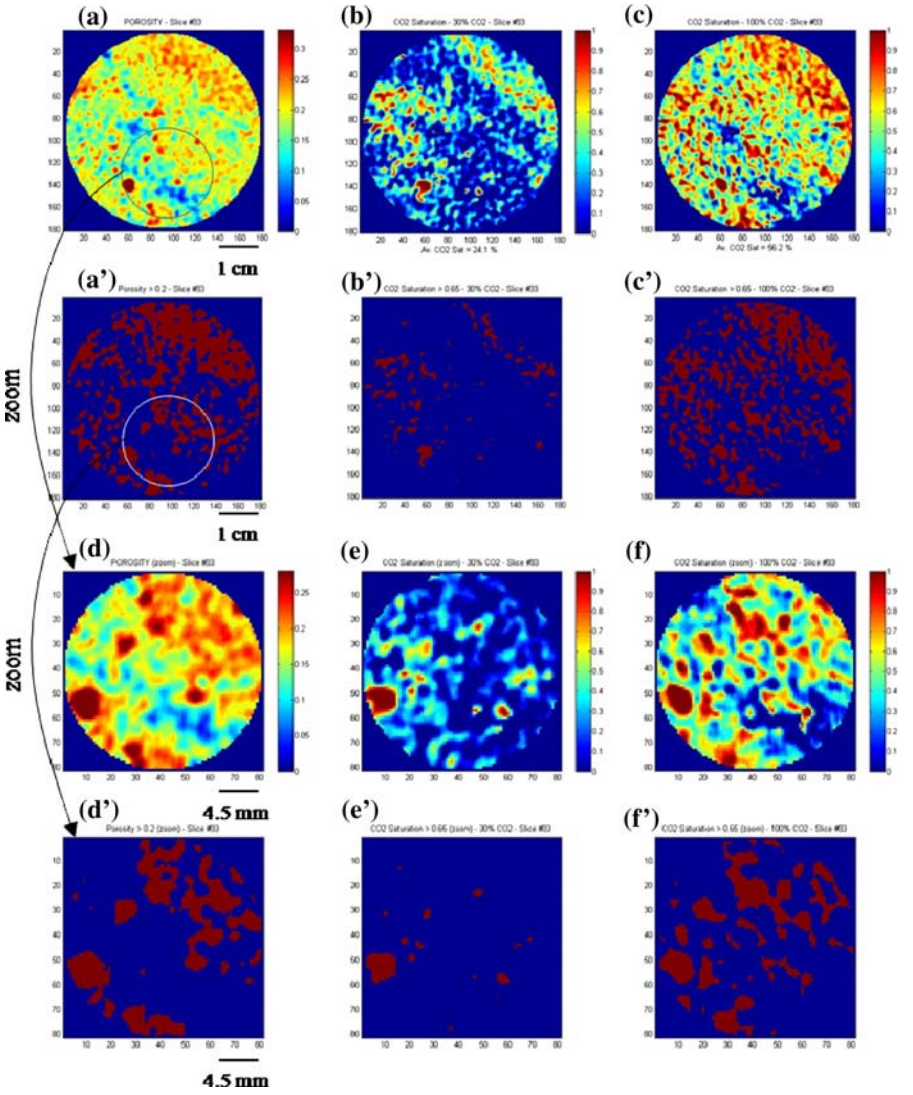

Fig. 8 **a** Porosity of slice #33. **b** and **c** CO_2 saturation of slice #33 corresponding, respectively, to the $f_{CO_2} = 0.3$ and $f_{CO_2} = 1$ cases. **a**′, **b**′, and **c**′ are the same images as **a**, **b**, and **c**, in a color scale that represents, in *red*, the values of porosity >0.2 and of saturation >0.65. **d**, **e**, and **f** correspond to details of images **a**, **b**, and **c** and images **d**′, **e**′, and **f**′ to zooms of images **a**′, **b**′, and **c**′. The zoomed area is indicated by a circle in **a** and **a**′

core have such a great influence on the relative permeability curves, the use of these data in simulations is not recommended.

4 Discussion and Observations

Two series of two-phase flow experiments have been carried out using an experimental apparatus that allows the measurement of steady-state two-phase relative permeability curves

f_{CO_2}	S_{brine}	Pressure drop (kPa)	$k_{r,brine}$	$k_{r,CO2}$
0	1	15.106	1	0
0.05	0.861	29.378	0.514	0.002
0.20	0.823	33.584	0.379	0.009
0.30	0.803	34.274	0.325	0.014
0.50	0.765	32.274	0.246	0.025
0.60	0.732	28.620	0.222	0.034
0.70	0.722	25.655	0.186	0.044
0.80	0.650	23.442	0.136	0.055
0.85	0.586	16.003	0.149	0.086
0.95	0.549	9.866	0.081	0.157
1	0.444	2.688	0	0.608

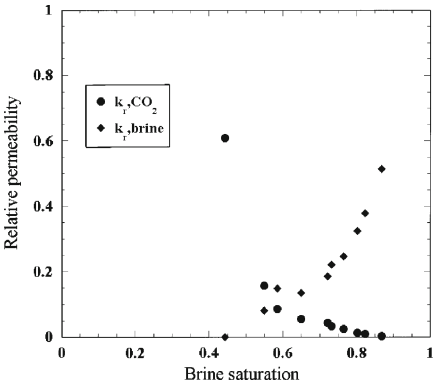

Fig. 9 Relative permeability data and curves measured during the drainage phase (sample #1) at 2 ml/min, 12.4 MPa and 63°C

Table 2 Sample properties and experimental conditions—sample #2

Sample properties	Experimental conditions	
Sample #2 (Berea sandstone)		
$\bar{\Phi} = 0.203$	$T_{res} = 50°C$	Brine composition: Na, 3,958 ppm; Cl, 6,109 ppm
$\bar{k} = 430 \pm 7$mD	$P_{res} = 12.4$ MPa	
$L = 15.24$ cm		
$\emptyset = 5.08$ cm		
Experiment 1 sample #2 (a)	Voxel size = 0.2539 × 0.2539 × 5.08 mm	Total flow rate: 1.2 ml/min (corresponding to a capillary number of $Ca \sim 1.8 \times 10^{-5}$ and a gravity number of $G = 0.296$)
Experiment 2 sample #2 (b)	Voxel size = 0.2539 × 0.2539 × 1 mm	Total flow rate: 1.7 ml/min (corresponding to a capillary number of $Ca \sim 2.6 \times 10^{-5}$ and a gravity number of $G = 0.210$)

at reservoir conditions. CO_2 saturation is determined using in situ X-ray CT scanning with a spatial resolution that allows studying the effect of sub-core scale heterogeneities in the samples. The porosity maps show that the two samples have significant heterogeneities in the porosity distribution. However, the connectivity between these heterogeneity features is clearly different, which leads to differences in brine displacement efficiency.

In sample #2, some high porosity layers are not connected to the inlet face of the core. This feature has a strong impact on fluid distribution as revealed by the 3D reconstructions of the saturation maps. Conversely, at the end of the drainage, the spatial distribution of CO_2 saturation in sample #1 is strongly correlated to the distribution of porosity in all the regions of the sample, high CO_2 saturations corresponding to high porosity. This indicates that all the regions of sample are accessible to CO_2 and thus that there is no capillary/permeability barrier that prevent the flow of CO_2. At the beginning of the drainage phase, the comparison between saturation and porosity clearly shows that CO_2 invades preferentially the high

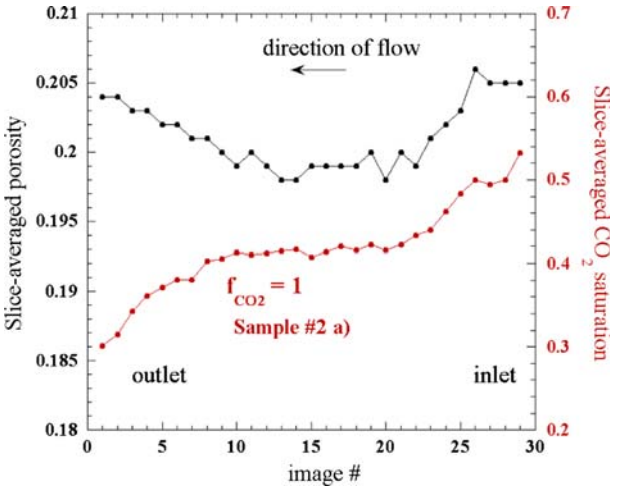

Fig. 10 Slice-averaged CO_2 saturation profile corresponding to the $f_{CO_2} = 1$ case in the experiment (a) and porosity profile

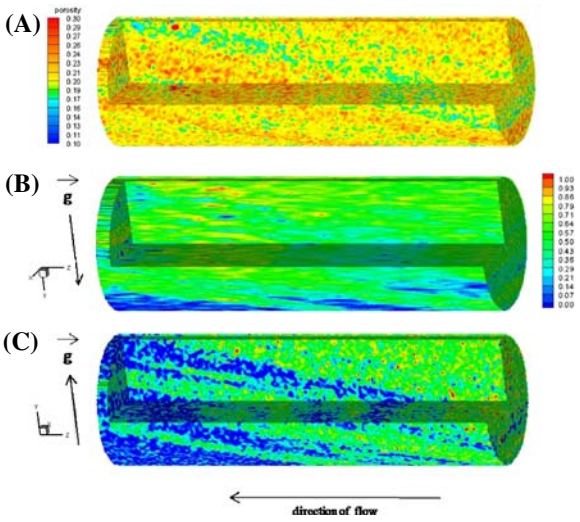

Fig. 11 3D reconstructions of porosity (*top*) and CO_2 saturation at $f_{CO_2} = 1$ for experiments (a) and (b). Note the different direction of the gravity vector for the two experiments, illustrating that spatial pattern of saturation is determined primarily by the rock properties, not gravity override of the CO_2. **a** Sample #2 porosity. **b** Sample #2 CO_2 saturation map (a) $f_{CO_2} = 1$, flow rate = 1.2 ml/min, Voxel size = 0.245 × 0.254 × 5.08 mm. **c** Sample #2 CO_2 saturation map (b) $f_{CO_2} = 1$, flow rate = 1.7 ml/min, Voxel size = 0.245 × 0.254 × 1 mm

porosity regions. In sample #2, the correlation is lost close to the outlet end of the core. This observation, which is usually attributed to a capillary end effect, is understood here as a result of the lack of connectivity between higher porosity layers and the inlet face of the core sample. The displacement efficiency is thus strongly limited by the heterogeneities and the residual brine saturation stays high.

At the flow rates that were used to perform the experiments, the results indicate that gravity does not play an important role because no evidence for spatial segregation exists between the top and the bottom halves of the samples that can be attributed to gravity override. Finally, the relative permeability curves both have high residual brine saturations that result partly from a general heterogeneity effect where CO_2 bypasses portions of the core with low porosity and higher capillary entry pressure and partly from the very specific orientation of the bedding as in sample #2.

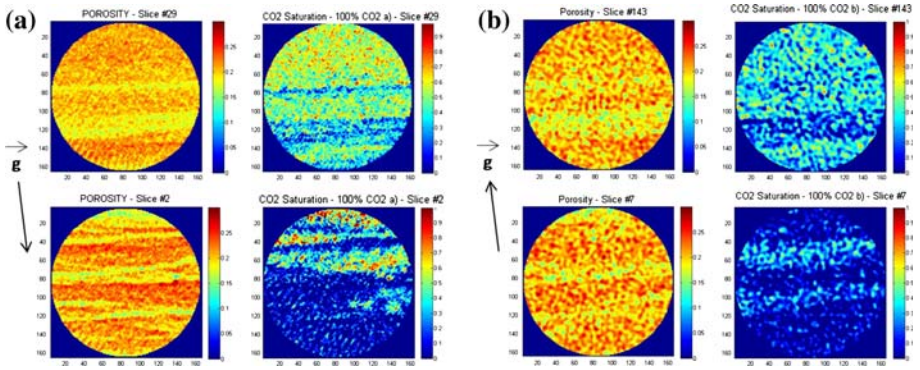

Fig. 12 Porosity and CO_2 saturation images at the inlet face and close to the outlet during experiments (a) and (b). The direction of gravity is indicated by an *arrow* in both cases

f_{CO_2}	S_{brine}	Pressure drop (kPa)	$k_{r,brine}$	$k_{r,CO2}$
0.26	0.95	3.034	0.445	0.019
0.34	0.87	5.274	0.234	0.015
0.51	0.79	5.757	0.172	0.023
0.61	0.77	5.343	0.154	0.030
0.79	0.73	5.481	0.09	0.042
1	0.62	4.447	0	0.063

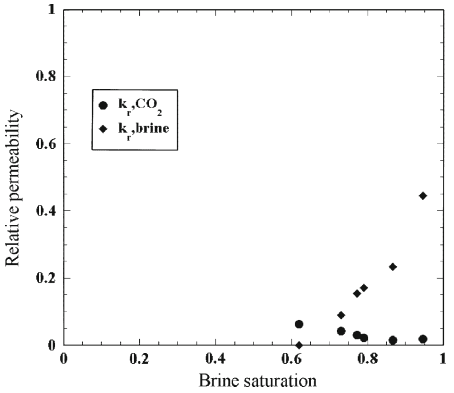

Fig. 13 Relative permeability to CO_2 and brine—experiment (b)—measured during the drainage phase. Sample #2(a) at 1.2 ml/min, 12.4 MPa and 50°C

In addition to the specific multi-phase flow behavior observed here, there are some general lessons and cautions that can be taken from these experiments.

The relative role of body forces (gravity) and viscous forces can be calculated using the dimensionless so-called gravity number: $G = \Delta\rho g k / U\mu$, where $\Delta\rho$ is the density difference between brine and CO_2, k is the mean permeability, U is the fluid velocity, and μ is the viscosity. In the case of the first experiment, the fluid velocity is high and the core permeability is low so that the value of the gravity number is low ($G = 0.033$). The viscous forces are dominant, as confirmed by our experiments. In the second case, the flow rate is lower and the permeability higher so that the gravity number is about 10 times higher than in the first experiment [experiment (a): $G = 0.296$; experiment (b): $G = 0.210$]. We find that even in this case with much higher gravity numbers, the distribution of CO_2 saturation at steady state is still controlled by structural heterogeneities, namely the low porosity layers oriented in the diagonal of the core. In the specific conditions in which the experiments have been performed, a simple calculation of the gravity number is thus not enough to get a precise idea of the flow regime. However, drilling plugs in the vertical direction would inevitably show a different behavior, with more pronounced gravity effects. It can be also noted that the cores used here are relatively short and that different behavior are expected at larger scale.

The relative permeability curves shown in this article present high residual brine saturations as a result of the specific orientation of the bedding with respect to the axis of flow and of a bypass of some portions of the cores. Similarly, high residual saturations have been reported in Bennion et al. (2006a,b,c). Heterogeneities with different orientations will inevitably lead to different relative permeability curves and saturation distributions. Since every reservoir will have its own unique heterogeneities, the orientation and nature of the heterogeneity must be considered on a case by case basis when making relative permeability measurements and extrapolating them to field-scale multiphase flow behavior. In particular, caution should be exercised in extrapolating one set of relative permeability measurements to other reservoirs. In fact, one can even imagine that the relative permeability curves that perform well for predicting the plume behavior during injection, where viscous forces leading to horizontal flow dominate, are not appropriate for the post-injection period where gravity forces and vertical flow are dominate. Most generally, relative permeability curves should be determined on a case by case basis as in the oil or gas reservoirs.

Finally, potential storage aquifers often have higher salinity as compared to the salinity used in the experiments. Typical reservoir values range between 10,000 and 250,000 ppm. The saline water minimizes the effect of clay swelling and prevents permeability changes that could impact saturation values. In our experiments, the salinity conditions of the reservoirs have not been matched but the clays have been stabilized when the core was fired at high temperature. It is also important to note that salinity impacts interfacial tension and relative permeability (Bachu and Bennion 2008).

5 Conclusions

Two-phase flow experiments with CO_2 and brine have been carried out on two rock samples, each with significant, but not unusual, heterogeneity. X-ray CT scanning was used to measure 3D CO_2 saturation distributions during a set of steady-state relative permeability measurements. The experiments demonstrated that saturation distributions correlated reasonably well with the porosity distribution, with higher porosity regions of the rock sample correlating with high CO_2 saturations and lower porosity regions with lower saturations. The inclusion of low porosity regions leads to bypass of portions of the core, which in turn results in a high residual saturation of brine when 100% CO_2 is injected into the core. The heterogeneous distribution of CO_2 is one possible explanation for the high residual saturations observed in many of the published CO_2/brine relative permeability measurements. This effect is further enhanced by the spatial distribution and orientation of the heterogeneities relative to the direction of flow. When low porosity layers are oriented parallel to the direction of flow, large portions of the rock can be bypassed if the low porosity layers acts as a capillary barrier that channels the flow in the high porosity layers. Relative permeability measurements with large residual brine saturations (>60%) may result from this kind of heterogeneity—and caution must be taken when using these measurements to simulate field-scale multi-phase flows of CO_2 and brine. Nevertheless, the results presented here demonstrate that small scale heterogeneities, particularly low porosity inclusions, can exert a large influence on brine displacement efficiency.

Acknowledgments This study is funded by GCEP, the Global Climate and Energy Project at Stanford University. Thanks are also due to all the CO2CRC participants (whose list can be seen at www.co2crc.com.au) for access to core from the Otway Basin Pilot Project.

References

Akin, S., Kovscek, A.R.: Computed tomography in petroleum engineering research. In: Akin, S., Kovscek, A.R. (eds.) Applications of X-Ray Computed Tomography in the Geosciences, vol. 215, pp. 23–38. Geological Society, London (2003) (Special Publications, 0305-8719/03/$15. © The Geological Society of London)

Bachu, S., Bennion, D.B.: Effects of in-situ conditions on relative permeability characteristics of CO_2-brine systems. Environ. Geol. **54**, 1707–1722 (2008)

Bennion, D.B., et al.: Relative Permeability Characteristics for Supercritical CO_2 Displacing Water in a Variety of Potential Sequestration Zones in the Western Canada Sedimendary Basin. SPE 95547 (2005)

Bennion, D.B., et al.: Dependence on Temperature, Pressure, and Salinity of the IFT and Relative Permeability Displacement Characteristics of CO_2 Injected in Deep Saline Aquifers. SPE 102138 (2006a)

Bennion, D.B., et al.: The Impact of Interfacial Tension and Pore Size Distribution/Capillary Pressure Character on CO_2 Relative Permeability at Reservoir Conditions in CO_2-Brine Systems. SPE 99325-MS (2006b)

Bennion, D.B., et al.: Spercritical CO_2 and H_2S-Brine Drainage and Imbibition Relative Permeability Relationships for Intergranular Sandstone and Carbonate Formations. SPE 99326 (2006c)

Benson, S.M., et al.: Core Scale and Pore Scale Studies of Carbon Dioxide Migration in Saline Formations. In: Proceedings of 8th International Conference on Greenhouse Gas Control Technologies, IEA Greenhouse Gas Program, Trondheim, Norway (2006)

Caruana, A., Dawe, R.A.: Flow behaviour in the presence of wettability heterogeneities. Trans. Porous. Med. **25**, 217–233 (1996)

Crotti, M.A., et al.: Relative Permeability Curves: The influence of Flow Direction and Heterogeneities. Dependence of End Point Saturations on Displacement Mechanisms. SPE 39657 (1998)

Honarpour, M., Koederitz, L., Harvey, A.H.: Relative Permeability of Petroleum Reservoir. CRC Press, Boca Raton, Florida, USA (1986). ISBN 0-8493-5739-X

Huppler, H.D.: Numerical Investigation of the Effects of Core Heterogeneities on Waterflood Relative Permeability, vol. 249, p. 381. AIME (1970)

Perrin, J.-C. et al.: Core-scale experimental study of relative permeability properties of CO_2 and brine in reservoir rocks. Energy Procedia **1**(1), 3515–3522 (2009)

Schembre, J.M., Kovscek, A.R.: A technique for measuring two-phase relative permeability in porous media via X-ray CT measurements. J. Pet. Sci. Eng. **39**, 159–174 (2003)

Shi, J.-Q. et al.: History matching of CO_2 core flooding CT scan saturation profiles with porosity dependant capillary pressure. Energy Procedia **1**(1), 3205–3211 (2009)

Tetsuya, S. et al.: Geological storage of carbon dioxide by residual gas and solubility trapping. Int. J. Greenh. Gas Control **2**, 58–64 (2008)

Wellington, S.L., Vinegar, H.J.: X-ray computerized tomography. J. Pet. Technol. **39**, 885–898 (1987)